Chemical Geology 380 (2014) 97–109

Contents lists available at ScienceDirect

Chemical Geology

journal homepage: www.elsevier.com/locate/chemgeo

Iron isotope fractionation during crystallization and sub-solidus re-equilibration: Constraints from the Baima mafic layered intrusion, SW China

Lie-Meng Chen [a,b], Xie-Yan Song [b,*], Xiang-Kun Zhu [a,**], Xiao-Qi Zhang [b], Song-Yue Yu [b], Jun-Nian Yi [b]

[a] Laboratory of Isotope Geology, Ministry of Land and Resources, Institute of Geology, Chinese Academy of Geological Sciences, Beijing 100037, PR China
[b] State Key Laboratory of Ore Deposit Geochemistry, Institute of Geochemistry, Chinese Academy of Sciences, Guiyang 550002, PR China

ARTICLE INFO

Article history:
Received 28 November 2013
Received in revised form 20 April 2014
Accepted 25 April 2014
Available online 2 May 2014

Editor: David R. Hilton

Keywords:
Iron isotopes
Isotope fractionation
Baima intrusion
Magmatic crystallization
Sub-solidus re-equilibration

ABSTRACT

To better understand Fe isotope fractionation between mafic minerals and oxides during crystallization of mafic magma and sub-solidus re-equilibration, the Fe isotopes of whole-rocks and separated minerals (olivine, clinopyroxene, magnetite and ilmenite) of the Baima mafic layered intrusion, SW China, have been investigated. The separated minerals show a systematical decrease in $\delta^{57}Fe$ values, from magnetite (0.15 to 0.51‰) to olivine (−0.11 to 0.15‰) and clinopyroxene (−0.35 to 0.05‰) and then to ilmenite (−0.82 to −0.10‰), demonstrating regular fractionation between these minerals. Except for a few of samples, most of the olivine and clinopyroxene are similar to those of mantle xenoliths in Fe isotopes, indicating that Fe isotope equilibrium reached during magma crystallization was well preserved. By contrast, the Fe isotopes of the magnetite and ilmenite may be evidently modified by sub-solidus re-equilibration via the Fe^{3+} versus Ti^{4+} and Fe^{2+} exchange between the oxides. Furthermore, the sub-solidus re-equilibration in Fe isotope is strongly controlled by the proportions of magnetite and ilmenite in rocks. Therefore, although the $\delta^{57}Fe_{Ilm}$ of the Lower Zone rocks with magnetite/ilmenite ratios as high as 6–10 was reduced evidently by the sub-solidus re-equilibration, the magnetite preserved their original Fe isotope compositions. By contrast, the Fe isotopes of both most magnetite and ilmenite in the Middle Zone had been markedly modified by sub-solidus re-equilibration owing to the moderate magnetite/ilmenite ratios (4–7). The decreases of both $\delta^{57}Fe_{Mt}$ and $\delta^{57}Fe_{Ol}$ upwards in the cyclic units of the Lower Zone reveal that extensive early fractional crystallization of the magnetite resulted in depletion of heavier Fe isotopes in the magma. On the other hand, early crystallization of olivine and clinopyroxene gave rise to the slight elevation of $\delta^{57}Fe_{Ol}$ values upwards in the cyclic units of the Middle and Upper zones. The stratigraphic reversals in the $\delta^{57}Fe_{Mt}$ and $\delta^{57}Fe_{Ol}$ values suggest multiple magma recharges. Additionally, the $\delta^{57}Fe_{Ol}$ values in the base of the Lower Zone (0.10 to 0.15‰) indicate that the parental magma were heavy in Fe isotope due to extensive silicate mineral fractionation at depth. This study indicates fractionation in Fe isotope between silicates and oxides during magma crystallization and sub-solidus re-equilibration.

1. Introduction

Iron isotopes are one of the most important non-traditional stable isotope systems to address petrogenetic issues because of high abundance and variable oxidation states of iron. The magnitude of Fe isotope fractionation strongly decreases with increasing temperature (Urey, 1947) and thus had been considered to be negligible between minerals in igneous rocks (e.g. Beard and Johnson, 1999). However, recent high-precision measurements have verified that significant Fe isotope fractionation may occur not only during mantle partial melting (e.g. Williams et al., 2005, 2009; Weyer and Ionov, 2007; Dauphas et al., 2009; Poitrasson et al., 2013; Teng et al., 2013), but also during magma fractional crystallization (Teng et al., 2008; Schoenberg et al., 2009; Sossi et al., 2012; Wang et al., 2012; Weyer and Seitz, 2012). Teng et al. (2008) and Weyer and Seitz (2012) showed that olivine phenocrysts are lighter in Fe isotope than their host basalts, which became heavier in Fe isotope with decrease of MgO due to fractional crystallization of olivine. Recently, the magnetite was reported to be significantly enriched in heavy Fe isotope relative to the pyroxene in the Red Hill

* Correspondence to: X.-Y. Song, Institute of Geochemistry, Chinese Academy of Sciences, 46th Guanshui Road, Guiyang 550002, PR China. Tel.: +86 851 5895538; fax: +86 851 5891664.
** Correspondence to: X.-K. Zhu, Institute of Geology, Chinese Academy of Geological Sciences, 26th Baiwanzhuang Street, Beijing 100037, PR China. Tel./fax: +86 10 68999798.
E-mail addresses: songxieyan@vip.gyig.ac.cn (X.-Y. Song), xiangkun@cags.ac.cn (X.-K. Zhu).

http://dx.doi.org/10.1016/j.chemgeo.2014.04.020
0009-2541/

doleritic intrusion, Southern Tasmania (Sossi et al., 2012) and the Panzhihua gabbroic intrusion, SW China (Wang, 2013). Additionally, abnormal Fe isotope compositions of some minerals were attributed to kinetically chemical diffusion during crystallization (e.g. Teng et al., 2008, 2011; Richter et al., 2009a,b; Dziony et al., 2014). Whether or not Fe isotope compositions of the Fe-bearing minerals in igneous rocks could be modified by sub-solidus re-equilibration has not been addressed.

On the other hand, systematic measurements on Fe isotope compositions of all Fe-bearing minerals of an intrusion or a volcanic suite are very rare. Except for several ilmenite grains in drilled rocks from IODP Hole 1256D (eastern equatorial Pacific, Dziony et al., 2014), few Fe isotopic data of ilmenites, one of the most important oxides in igneous rocks, have not been reported in previous literatures. This means that the Fe isotope fractionation between Fe-bearing minerals along with magma differentiation has been only partially revealed. Therefore, knowledge on the mechanisms and critical factors that govern Fe isotope fractionation between Fe-bearing minerals during fractional crystallization and sub-solidus re-equilibration are still very limited, particularly for a layered intrusion in a magma plumbing system. The well-characterized lithologically zoned Baima mafic layered intrusion at the central Emeishan Large Igneous Province (ELIP) is ideal for examining these issues. Recent petrology and geochemistry studies have indicated that the Baima intrusion was formed by accumulation of Fe–Ti oxides and silicate minerals crystallized from repeatedly replenished Fe–Ti-enriched magmas, which were generated by fractional crystallization of chromite, olivine, and pyroxene from a high-Ti picritic magma at deep level (Zhang et al., 2012, 2013). In this study, we present the Fe isotopic systematics of the whole-rocks and separated minerals, including magnetite, ilmenite, olivine, and clinopyroxene, from the Baima intrusion. These data, combined with major and trace element compositions of the whole rocks and minerals, permit us to reveal the dominated mechanisms leading to Fe isotope fractionation between minerals. We also evaluate the variations of the Fe isotope of magnetite and ilmenite resulted from sub-solidus re-equilibration Fe^{3+} versus Fe^{2+} and Ti^{4+} exchange between them. The potential petrogenetic implications of the Fe isotope compositions of these minerals are discussed as well.

2. Geological background and petrography of the Baima intrusion

The ELIP is consisted of the Late Permian continental flood basalts wide-spreading over an area of 5×10^5 km^2 and genetically associated mafic–ultramafic intrusions and felsic alkaline plutons, which are believed to be derived from a mantle plume, in the western Yangtze Block, SW China (Chung and Jahn, 1995; Song et al., 2001, 2004, 2008, 2009; Xu et al., 2001, 2004; Zhou et al., 2002; Ali et al., 2005; Zhang et al., 2006). Several large mafic–ultramafic layered intrusions, including Taihe (She et al., 2014), Baima (Zhang et al., 2012, 2013), Panzhihua (Zhou et al., 2005; Pang et al., 2008a,b; Song et al., 2013), Hongge (Bai et al., 2012; Luan et al., 2014) and Xinjie (Zhong et al., 2004, 2011), occur in the central part of the ELIP along N–S trending faults (Fig. 1; Panxi Geological Unit, 1984). Most of the intrusions have been dated at ~260 Ma (Zhou et al., 2002, 2008; Zhong and Zhu, 2006; Zhong et al., 2007; Shellnutt et al., 2012). Periodical replenishment of fractionated and Fe–Ti-enriched mafic magmas from deep-seated magma chambers resulted in the formation of Fe–Ti oxide ore layers in the lower and/or middle zones of these intrusions (Zhang et al., 2012; Song et al., 2013; Luan et al., 2014; She et al., 2014).

The N–S striking Baima layered intrusion is ~24 km long and ~2 km thick and dips 50–70° to the west. It was emplaced into the Sinian metasandstone, marble, phyllite and slate and in turn was intruded and surrounded by the late Permian syenite and granite (Fig. 1, Panxi Geological Unit, 1984). The intrusion was subdivided into five segments including Xiajiaping, Jijiping, Tianjiacun, Qinggangping and Mabinlang from north to south by a series of NE–SW-trending faults (Fig. 1). According to mineral assemblages and lithologic textures, the Baima intrusion can be subdivided into Basal Zone, Lower Zone (LZ), Middle Zone (MZ), and Upper Zone (UZ) from the base upwards (Fig. 1; Panxi Geological Unit, 1984; Zhang et al., 2012).

The Basal Zone consists of pegmatitic gabbro. The LZ is remarkable by significant high proportions of Fe–Ti oxides and consists of magnetite wehrlite and magnetite troctolite and a few interlayers of troctolite and gabbro. The magnetite wehrlite contains as high as 45–55 modal % magnetite, 5–8% ilmenite, 15–30% olivine, 10–20% clinopyroxene and plagioclase, and minor hornblende and sulfides (Fig. 2a). Aggregations of the silicate minerals are insulated by matrix of the oxides in the magnetite wehrlite. The ilmenite grains occur between the larger magnetite grains (Fig. 2a). The magnetite troctolite contains less Fe–Ti oxides (20–40% magnetite, and <5% ilmenite) and more silicate minerals (30–40% olivine, 20–30% plagioclase, and <15% clinopyroxene; Panxi Geological Unit, 1984; Zhang et al., 2012). Based on the compositional reversals of the olivine and plagioclase and whole-rock Cr contents, Zhang et al. (2012) subdivided the LZ into six cyclic units, I to VI from the base upward (Fig. 1), indicating several pulses of magma injection during the formation of the LZ. The magnetite/ilmenite ratios of the LZ rocks are as high as 5.8–10.3 and generally decrease from the base to the top of each cyclic unit (Fig. 1), suggesting crystallization of the magnetite earlier than the ilmenite. The higher forsterite percentages of the olivine (Fo = 65–74%) and anorthite contents of the plagioclase (An = 56–67%) of the LZ rocks relative to those of the MZ (Fo = 55–67%, An = 56–58%) and UZ (Fo = 55–61%) rocks indicate that the parental magmas of the LZ were more primitive (Fig. 1).

The MZ, equal to the Upper Zone of Zhang et al. (2012), dominantly comprises of troctolite and olivine gabbro. The troctolite contains ~50–60% plagioclase, ~10–20% olivine, <10% clinopyroxene, and <20% Fe–Ti oxides. The olivine gabbro differs from the troctolite in having a higher proportion of clinopyroxene (~10–20%) and lower olivine (<10%) (Fig. 2b). They are low in magnetite/ilmenite ratios (3.9–6.8) relative to the LZ rocks (Figs. 1, 2b). The MZ can be subdivided into two thick cyclic units (VII and VIII). In the cyclic unit VII, Fo of the olivine and An of the plagioclase decrease upwards (Fig. 1). It is notable that the rocks of the cyclic unit VII have lower contents of $Fe_2O_{3(T)}$ and TiO_2 than the troctolite of the cyclic unit VIII as well as some of the UZ rocks (Fig. 1). This means that the rocks of the cyclic unit VII contain less Fe–Ti oxides. Crystallization and accumulation of plagioclase and mafic silicates from the mixture of the new replenished magma and residual melt of the LZ produced the MZ troctolite and gabbro (Zhang et al., 2012). Regularly oriented exsolution lamellae of magnetite are common in the clinopyroxene crystals of the LZ and MZ rocks, implying that the replenished magmas are Fe–Ti enriched. Moreover, the Fe–Ti oxides have experienced significantly sub-solidus re-equilibration as shown by abundance of exsolution lamellae of ilmenite in the magnetite crystals (Zhang et al., 2012).

The UZ is marked by a sudden appearance of cumulate apatite and consists of apatite olivine gabbro and apatite gabbro. It is further subdivided into cycle unit IX and X, with decreasing of olivine contents upward for each unit. The UZ rocks are composed of plagioclase (40–60%), clinopyroxene (20–40%), Fe–Ti oxides (~10–20%), olivine (~5–10%), apatite (~3–5%) and trace amounts of sulfides and biotite (Fig. 2c). Subhedral to euhedral olivine crystals are poikilitically enclosed by plagioclase and clinopyroxene. A particularly important feature to note is that the ilmenite is subequal to magnetite in the UZ rocks, showing the lowest ratios of magnetite/ilmenite (1.1–3.7) relative to the LZ and MZ (Figs. 1, 2c). The low Fo values of the olivine and appearance of apatite in the UZ rocks, as well as the low ratios of magnetite/ilmenite (1.1–3.7) and whole-rock Fe^{3+}/Fe^{2+} (0.23–0.39), indicate that the apatite gabbro was formed by more evolved magmas under a relatively lower oxygen fugacity (Fig. 1; Zhang et al., 2012). The decreases of the magnetite/ilmenite ratios from the lower zone to upper zone have been also observed in the Panzhihua gabbroic intrusion (Howarth et al., 2013; Song et al., 2013).

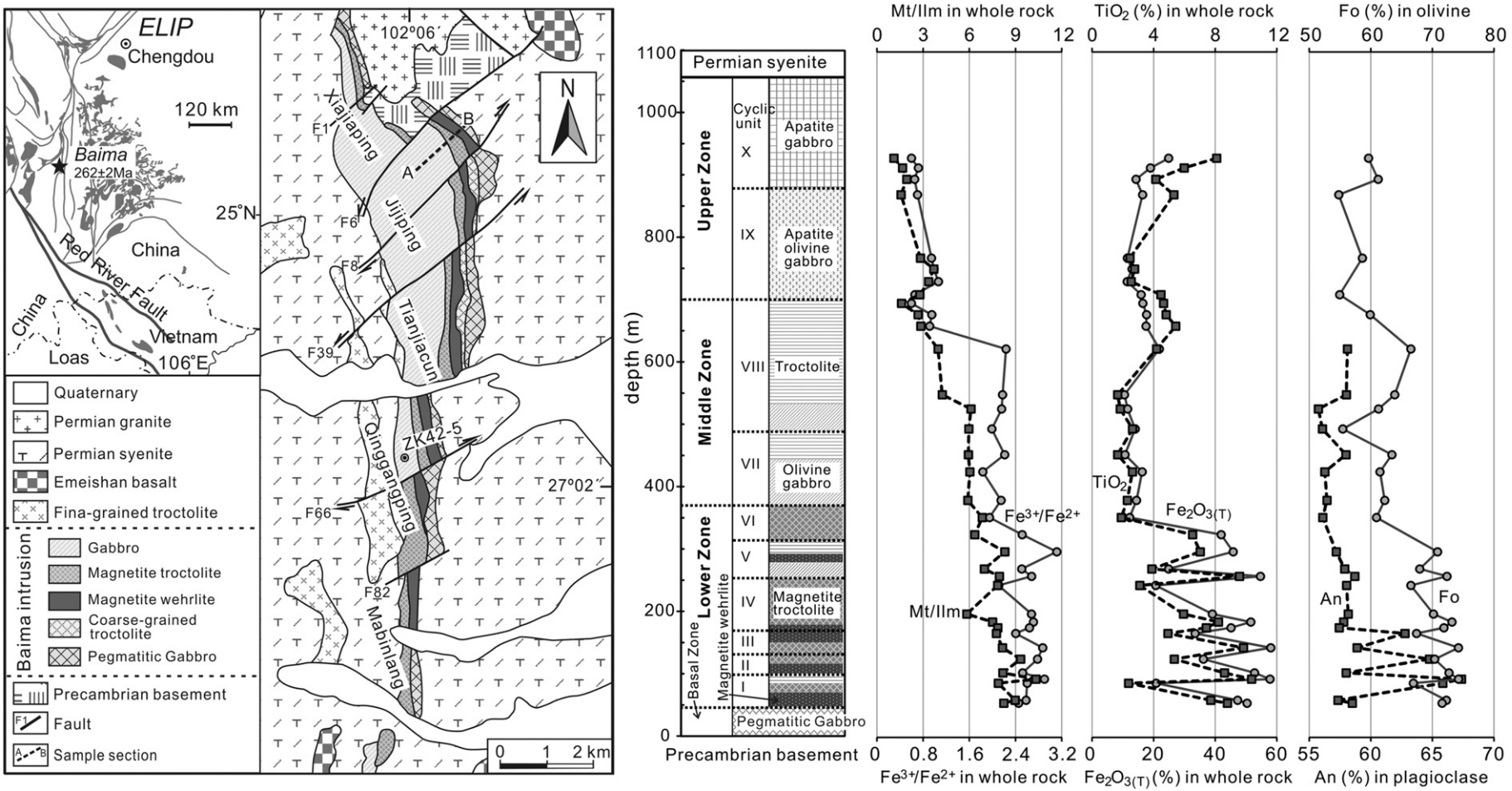

Fig. 1. Simplified geological map of the Emeishan Large Igneous Province (ELIP, modified after Zhou et al., 2002, 2008 and Song et al., 2009, 2013), the Baima layered intrusion (modified after Panxi Geological Unit, 1984, and Zhang et al., 2012) and simplified stratigraphic column of the Baima intrusion of combination with the Jijiping and Qinggangping segments. The zonal subdivision, proportions of magnetite (Mt) and ilmenite (Ilm), and compositional variations of the whole rocks, olivine, and plagioclase of the Jijiping segment are after Zhang et al. (2012). These data of the Qinggangping segment are from our unpublished data.

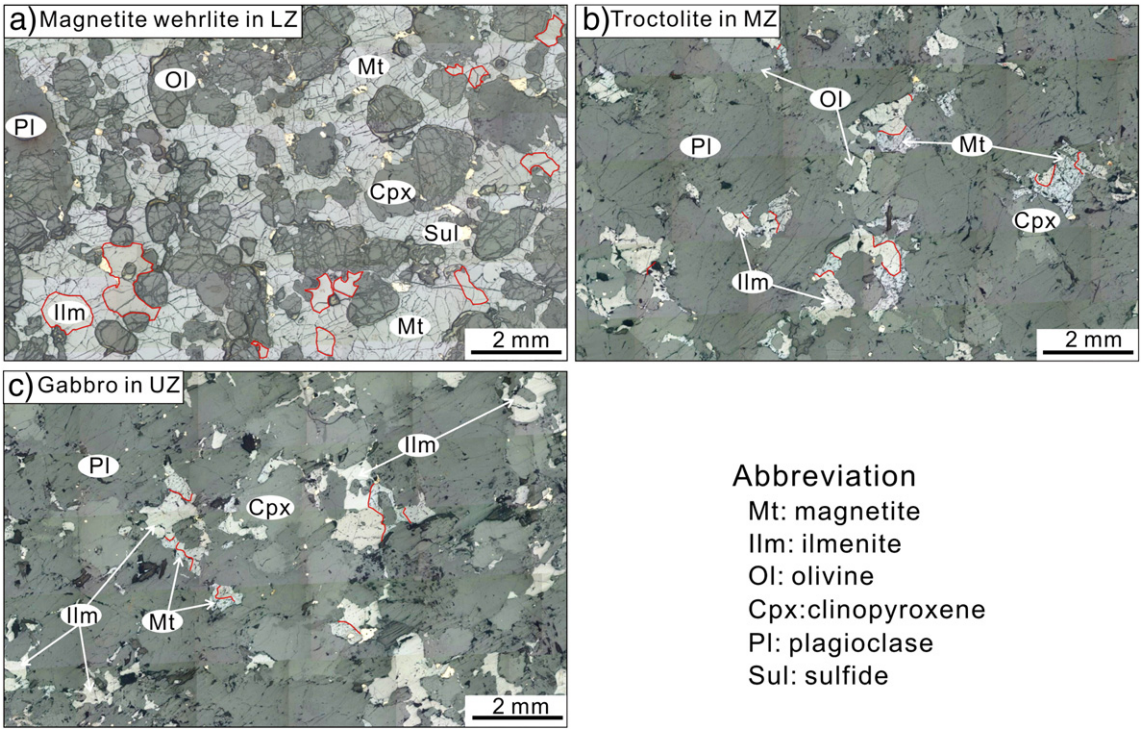

Fig. 2. Microphotographs showing magnetite and ilmenite textures of the Baima layered intrusion. (a) Magnetite wehrlite in LZ showing much greater Mt/Ilm ratio; (b) Troctolite in MZ showing slightly higher Mt/Ilm ratio; and (c) Gabbro in UZ showing low Mt/Ilm ratio.

3. Sampling and analytical techniques

Twenty representative samples were collected from the LZ to the middle part of the MZ at the Jijiping segment (Fig. 1). Eleven samples of the UZ were selected from exploration bore hole (ZK42-5) at the Qinggangping segment, because the UZ is not outcropped well along the Jijiping segment (Fig. 1).

Samples were crushed to 60 to 100 meshes; oxides and silicates were separated roughly using magnetic separator. Then, the magnetite, ilmenite, olivine and clinopyroxene were handpicked carefully under binocular microscope. In order to avoid contamination from magnetite inclusions enclosed in clinopyroxene, only the transparent brown crystals were selected for Fe isotope measurement. The separated minerals had been tested using Electronic Microprobe in the Institute of Geochemistry, Chinese Academy of Sciences. The purity of the separated mineral is better than 95%. The individual grains were cleaned ultrasonically three times in purified Milli-Q water (18.2 MΩ) for 10 min.

Iron isotope analysis was determined using Nu Plasma HR MC–ICP–MS at the Laboratory of Isotope Geology (LIG), Institute of Geology, Chinese Academy of Geological Sciences. Procedures for sample preparation and instrumental analysis are similar to those described in Zhu et al. (2002, 2008) and Wang et al. (2011). Total procedural iron blanks were always below 10 ng, which is considered negligible compared to the amounts of iron processed (~20 μg).

Iron isotope is reported relative to the international isotopic reference standard IRMM-014: $\delta^{X}Fe = [(^{X}Fe/^{54}Fe)_{sample}/(^{X}Fe/^{54}Fe)_{IRMM\text{-}014} - 1.0] \times 10^{3}$ (‰), where X = 56 or 57. The long-term external reproducibility for $\delta^{57}Fe$ and $\delta^{56}Fe$ are better than 0.1‰ at 2 SD level estimated from repeated measurements of in-laboratory standard solution (CAGS-Fe) and national basaltic standard reference GBW07105 against IRMM-014 (Zhu et al., 2008; Tang et al., 2012). Both the

Table 1
Comparisons of Fe isotope of standards measured in this study with literature data.

Reference	BCR-2		GBW 07105	
	$\delta^{57}Fe \pm 2sd$	$\delta^{56}Fe \pm 2sd$	$\delta^{57}Fe \pm 2sd$	$\delta^{56}Fe \pm 2sd$
This study	0.12 ± 0.07	0.09 ± 0.04	0.21 ± 0.08	0.14 ± 0.04
Sossi et al. (2012)	0.14 ± 0.09	0.09 ± 0.07		
Craddock and Dauphas (2011)	0.13 ± 0.02	0.09 ± 0.01	0.23 ± 0.03	0.15 ± 0.02
Huang et al. (2011)		0.09 ± 0.04		
Dauphas et al. (2009)	0.13 ± 0.03	0.09 ± 0.03		
Wombacher et al. (2009)	0.12 ± 0.05	0.09 ± 0.06		
Dauphas et al. (2004)	0.16 ± 0.21	0.06 ± 0.08		
Tang et al. (2012)			0.19 ± 0.03	0.13 ± 0.04

sd = standard deviation.

Table 2
Fe isotopic compositions (per mil) of whole rocks, magnetite, ilmenite, olivine, and clinopyroxene and their associated uncertainties.

Zone	Cyclic unit	Sample No.	Rock type	Height* (m)	Whole rock					Magnetite			
					N	δ^{57}Fe	2SE	δ^{56}Fe	2SE	N	δ^{57}Fe	2SE	δ^{56}Fe	2SE
		SB11-52	Apat-Gabbro	1014	2	0.01	0.09	0.04	0.06	2	0.51	0.01	0.36	0.02
		SB11-58	Apat-Gabbro	997	2	0.11	0.12	0.08	0.03	2	0.48	0.04	0.32	0.04
		SB11-59	Apat-Gabbro	977	5	0.10	0.05	0.09	0.02	2	0.49	0.07	0.32	0.05
	X	SB11-81	Apat-Gabbro	950	2	−0.08	0.00	−0.01	0.04	2	0.31	0.05	0.23	0.01
		SB11-69	Apat-Ol-Gabbro	839	2	0.00	0.08	−0.02	0.02	4	0.47	0.05	0.31	0.05
		SB11-68	Apat-Ol-Gabbro	820	2	−0.07	0.05	−0.02	0.00	2	0.38	0.10	0.21	0.01
		SB11-68**			2	0.17	0.05	0.10	0.04	2	0.42	0.05	0.30	0.03
		SB11-57	Apat-Ol-Gabbro	775	2	−0.02	0.07	0.00	0.01	5	0.46	0.06	0.29	0.03
		SB11-64	Apat-Ol-Gabbro	760	2	0.07	0.09	0.03	0.05	2	0.33	0.07	0.22	0.06
		SB11-65	Apat-Ol-Gabbro	740	2	0.12	0.03	0.09	0.01	3	0.42	0.07	0.29	0.06
Upper zone	IX	SB11-100	Apat-Ol-Gabbro	720	2	0.18	0.01	0.10	0.01	3	0.41	0.08	0.29	0.02
		SB09-39	Troctolite	680	2	0.15	0.09	0.13	0.06	5	0.27	0.05	0.18	0.04
		SB09-37	Troctolite	575	5	0.19	0.07	0.15	0.05	3	0.34	0.05	0.27	0.03
		SB09-32	Troctolite	540	3	0.19	0.08	0.09	0.05	3	0.21	0.06	0.15	0.05
	VIII	SB09-31	Ol-Gabbro	495	2	0.13	0.09	0.09	0.03	2	0.26	0.03	0.21	0.02
		SB09-30	Troctolite	465	2	0.13	0.08	0.10	0.04	5	0.43	0.05	0.30	0.03
		SB09-29	Ol-Gabbro	415	4	0.10	0.04	0.06	0.07	2	0.46	0.02	0.30	0.02
Middle zone	VII	SB09-28	Ol-Gabbro	385	5	0.07	0.04	0.07	0.05	2	0.42	0.01	0.29	0.01
		SB09-27	Mt-Troctolite	355	4	0.13	0.10	0.11	0.07	2	0.22	0.04	0.13	0.05
		SB09-27**												
	VI	SB09-25	Mt-Troctolite	325	2	0.10	0.01	0.09	0.01	2	0.28	0.05	0.19	0.06
		SB09-24	Troctolite	295	2	0.17	0.03	0.09	0.05	2	0.25	0.05	0.21	0.05
	V	SB09-20	Ol-Gabbro	266	3	0.15	0.02	0.12	0.06	2	0.16	0.03	0.13	0.11
		SB09-20**												
		SB09-19	Mt-Troctolite	216	2	0.09	0.03	0.07	0.04	2	0.15	0.13	0.11	0.04
		SB09-18	Mt-Troctolite	202	2	0.07	0.05	0.07	0.01	2	0.24	0.14	0.18	0.07
		SB09-18**								2	0.17	0.11	0.10	0.05
		SB09-17	Mt-Troctolite	192	2	0.12	0.15	0.08	0.08	2	0.16	0.05	0.11	0.07
	IV	SB09-16	Mt-Troctolite	182	4	0.16	0.05	0.14	0.06	3	0.36	0.02	0.26	0.01
		SB09-15	Mt-Wehrlite	157	2	0.13	0.12	0.11	0.11	2	0.21	0.13	0.15	0.04
	III	SB09-14	Mt-Troctolite	137	3	0.29	0.05	0.16	0.04	3	0.28	0.05	0.20	0.08
		SB09-13	Mt-Troctolite	113	2	0.20	0.08	0.10	0.02	2	0.26	0.04	0.17	0.03
	II	SB09-11	Mt-Wehrlite	102	3	0.27	0.06	0.16	0.04	2	0.29	0.14	0.18	0.08
Lower zone	I	SB09-08	Mt-Wehrlite	60	3	0.13	0.02	0.13	0.02					

Sample No.	Ilmenite					Olivine					Clinopyroxene				
	N	δ^{57}Fe	2SE	δ^{56}Fe	2SE	N	δ^{57}Fe	2SE	δ^{56}Fe	2SE	N	δ^{57}Fe	2SE	δ^{56}Fe	2SE
SB11-52	2	−0.14	0.01	−0.09	0.03	2	0.04	0.10	0.03	0.09	2	0.00	0.03	−0.01	0.04
SB11-58															
SB11-59	2	−0.10	0.08	−0.05	0.04	2	0.02	0.07	0.05	0.01	5	−0.12	0.07	−0.08	0.04
SB11-81						2	−0.03	0.05	0.01	0.08	2	−0.15	0.03	−0.08	0.01
SB11-69	2	−0.21	0.09	−0.16	0.01	5	0.05	0.04	0.02	0.04	2	−0.04	0.13	−0.04	0.14
SB11-68	2	−0.18	0.03	−0.12	0.04	2	−0.11	0.07	−0.06	0.02	5	−0.04	0.05	−0.02	0.06
SB11-68**															
SB11-56															
SB11-57	2	−0.18	0.02	−0.11	0.03	2	0.00	0.03	−0.02	0.03	2	−0.25	0.03	−0.20	0.04
SB11-64	2	−0.12	0.02	−0.08	0.03	2	−0.05	0.10	−0.06	0.03	2	0.00	0.00	0.00	0.03
SB11-65						2	−0.08	0.02	−0.02	0.02					
SB11-100						2	0.00	0.09	0.00	0.01					
SB09-39															
SB09-37						4	−0.02	0.04	−0.03	0.04	2	−0.05	0.12	−0.04	0.08
SB09-32	2	−0.64	0.04	−0.46	0.05	3	−0.13	0.04	−0.10	0.06	4	−0.35	0.04	−0.22	0.05
SB09-31															
SB09-30	2	−0.30	0.12	−0.21	0.11						4	−0.07	0.08	−0.11	0.05
SB09-29	5	−0.42	0.09	−0.28	0.08	2	−0.07	0.03	−0.06	0.02	2	−0.18	0.06	−0.12	0.13
SB09-28	3	−0.40	0.11	−0.28	0.08						2	−0.08	0.06	−0.07	0.03
SB09-27	2	−0.35	0.13	−0.22	0.08	2	−0.06	0.14	−0.01	0.15	3	−0.13	0.07	−0.09	0.05
SB09-27**	2	−0.34	0.12	−0.19	0.11										
SB09-25	2	−0.30	0.12	−0.21	0.08	2	−0.06	0.09	−0.01	0.06	4	−0.06	0.03	−0.05	0.02
SB09-24															
SB09-20	2	−0.27	0.01	−0.18	0.04	2	−0.08	0.05	−0.03	0.01	2	−0.12	0.05	−0.08	0.07
SB09-20**						2	−0.03	0.04	−0.03	0.02	3	−0.13	0.08	−0.08	0.03
SB09-19	2	−0.37	0.07	−0.25	0.04	2	−0.04	0.05	−0.01	0.04	2	0.05	0.01	0.06	0.09
SB09-18	2	−0.37	0.07	−0.23	0.07	2	0.02	0.09	0.06	0.02	2	0.01	0.03	0.00	0.08
SB09-18**															
SB09-17	2	−0.43	0.07	−0.27	0.04	2	0.04	0.10	0.02	0.03					
SB09-16															

(continued on next page)

Table 2 (*continued*)

Sample No.	Ilmenite					Olivine					Clinopyroxene				
	N	δ^{57}Fe	2SE	δ^{56}Fe	2SE	N	δ^{57}Fe	2SE	δ^{56}Fe	2SE	N	δ^{57}Fe	2SE	δ^{56}Fe	2SE
SB09-15						4	0.10	0.03	0.07	0.06					
SB09-14	5	−0.82	0.09	−0.57	0.07						2	−0.02	0.07	−0.04	0.05
SB09-13	5	−0.70	0.06	−0.48	0.04	4	0.10	0.04	0.06	0.04	2	−0.22	0.11	−0.15	0.07
SB09-11	2	−0.36	0.12	−0.24	0.01	4	0.15	0.07	0.12	0.02	2	−0.27	0.05	−0.20	0.04
SB09-08															

*height from base; ** represent duplicate samples of different digestions; N denotes the number of repeated analyses by MC-IPC-MS; SE stands for standard error.
Abbreviations: Mt-Wehrlite = magnetite wehrlite; Mt-Troctolite = magnetite troctolite; Ol-Gabbro = olivine gabbro; Apat-Ol-Gabbro = apatite olivine gabbro; Apat-Gabbro = apatite gabbro.

international basaltic standard reference BCR-2 and GBW07105 were processed with unknown samples to control data quality. The measured Fe isotopic data show excellent agreement with previous literature values (Table 1). For some bulk rocks and mineral powders, two duplicates of each sample were processed and determined separately. All duplicated analyses exhibit good reproducibility (Table 2). Furthermore, on a three-isotope diagram, all Fe isotopic data define a single mass-dependent line with a slope of ~0.68 (Fig. 3).

4. Results

The Fe isotopic compositions of the whole-rocks, magnetite, ilmenite, olivine, and clinopyroxene are present in Table 2. Stratigraphic variations of them are illustrated in Fig. 4.

4.1. Stratigraphic variation of Fe isotope

Iron isotopes of the whole rocks and minerals have distinctive stratigraphic variations in the three lithologic zones (Fig. 4). In the LZ, the whole-rock δ^{57}Fe values vary from 0.07 to 0.29‰ and the mineral δ^{57}Fe values decrease systematically from magnetite (0.15 to 0.36‰), to olivine (−0.08 to 0.15‰) and clinopyroxene (−0.27 to 0.05‰), then to ilmenite (−0.82 to −0.30‰) (Table 2). In most of the cyclic units of this zone, the Fe isotopic compositions of magnetite and olivine as well as whole-rock become lighter regularly from the base upward, whereas the ilmenite and clinopyroxene have large variations in δ^{57}Fe (Table 2, Fig. 4). It is noticeable that the δ^{57}Fe values of the olivine in the cyclic units II and III are comparable with the average of the OIBs (~0.15‰; e.g. Beard et al., 2003; Teng et al., 2008, 2013; Schuessler et al., 2009) and obviously higher than those of most of the olivine in the other cyclic units (Fig. 4).

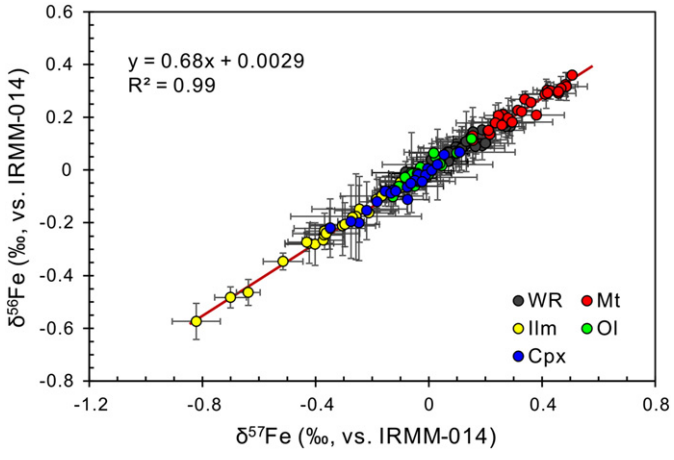

Fig. 3. Three isotope plot of Fe isotopes, showing that all the Fe-isotope data from both the whole rocks and minerals from the Baima layered intrusion plot on a single mass-fractionation line. The slope of δ^{57}Fe vs. δ^{56}Fe is 0.68, and $r^2 = 0.99$, consistent with the values calculated from equilibrium and kinetic mass dependent isotope fractionation line (Zhu et al., 2001; Young et al., 2002). Error bars given reflect 2SE in Table 2. Abbreviations: WR = whole rock, Mt = magnetite, Ilm = ilmenite, Ol = olivine, and Cpx = clinopyroxene.

In contrast to the LZ, the MZ rocks have narrow range of δ^{57}Fe values, which increase regularly from the base to the top for each cyclic unit, varying from 0.07 to 0.13‰ in the cyclic unit VII and from 0.13 to 0.18‰ in the cyclic unit VIII, respectively (Table 2, Fig. 4). Although the δ^{57}Fe values of the magnetite of the cyclic unit VIII (0.21 to 0.34‰) are similar to those of the LZ magnetite, those of the cyclic unit VII have higher $\delta^{57}Fe_{Mt}$ values (0.42 to 0.46‰) (Table 2, Fig. 4). On the other hand, the MZ ilmenite has Fe isotopic values similar to most of the LZ ilmenite, ranging from −0.64 to −0.30‰ (Table 2, Fig. 4). The MZ olivine has limited variations in δ^{57}Fe, displaying an increase upward in cyclic unit VIII. Similarly, the MZ clinopyroxene shows a small range of δ^{57}Fe values varying from −0.18 to −0.05‰ (except one sample as low as −0.35‰; Table 2, Fig. 4).

The UZ rocks are characterized by slightly lighter Fe isotopic values (−0.07 to 0.17‰ in δ^{57}Fe; Fig. 4). Comparing to the LZ and MZ, the UZ ilmenite shows the heaviest δ^{57}Fe values, varying from −0.21 to −0.10‰. On the contrary, the magnetite of the UZ has the δ^{57}Fe values (0.31 to 0.51‰) that are slightly higher than those of the LZ but similar to those of the MZ (Table 2, Fig. 4). The olivine and clinopyroxene show increase trends in δ^{57}Fe values upward in the cyclic units IX and X, respectively (Table 2, Fig. 4). The δ^{57}Fe values of the olivine crystals of the Baima intrusion are similar to those of the olivine phenocrysts in the Hawaii basalts (Teng et al., 2011).

4.2. Inter-mineral Fe isotope correlation

Except for four outliers (SB09-11, 13, 32 and 57), most of the Baima samples plot within the area of the mantle xenoliths in the binary diagram of $\delta^{57}Fe_{Ol}$ vs. $\delta^{57}Fe_{Cpx}$ and fall between the lines of $\Delta^{57}Fe_{Ol\text{-}Cpx}$ ($=\delta^{57}Fe_{Ol} - \delta^{57}Fe_{Cpx}$) equaling +0.1 and −0.1 with a slope of ~1 (Fig. 5a). In contrast, all of the Baima samples, except for the three LZ and MZ samples having extremely low $\delta^{57}Fe_{Ilm}$, show three trends below the line of $\Delta^{57}Fe_{Mt-Ilm} = 0$ in the diagram of $\delta^{57}Fe_{Mt}$ vs. $\delta^{57}Fe_{Ilm}$ (Fig. 5b). The LZ and UZ samples are characterized by the lowest $\delta^{57}Fe_{Mt}$ and the highest $\delta^{57}Fe_{Ilm}$, respectively, and the MZ samples have moderate $\delta^{57}Fe_{Mt}$ and $\delta^{57}Fe_{Ilm}$ values and show remarkable fractionation with $\Delta^{57}Fe_{Mt-Ilm}$ between 0.73 and 0.88‰ (Fig. 5b). Most of the LZ samples plot on a trend defined by a relatively small range of $\Delta^{57}Fe_{Mt-Ol}$ (0.11 to 0.24‰), whereas the MZ and UZ samples have higher $\delta^{57}Fe_{Mt}$ values (0.21 to 0.51‰) resulting in greater $\Delta^{57}Fe_{Mt-Ol}$ (0.27 to 0.49‰) (Fig. 5c). In addition, most of the LZ magnetite–clinopyroxene pairs plot near the trend of rocks from the Red Hill intrusion (Sossi et al., 2012) with $\Delta^{57}Fe_{Mt-Cpx}$ values of 0.22 to 0.35‰, whereas, the MZ and UZ samples have higher $\Delta^{57}Fe_{Mt-Cpx}$ ranging from 0.39 to 0.64‰ (Fig. 5d). The two LZ samples and one MZ sample, which show extremely low $\delta^{57}Fe_{Ilm}$ values, as well as one UZ sample display very low $\delta^{57}Fe_{Cpx}$ values.

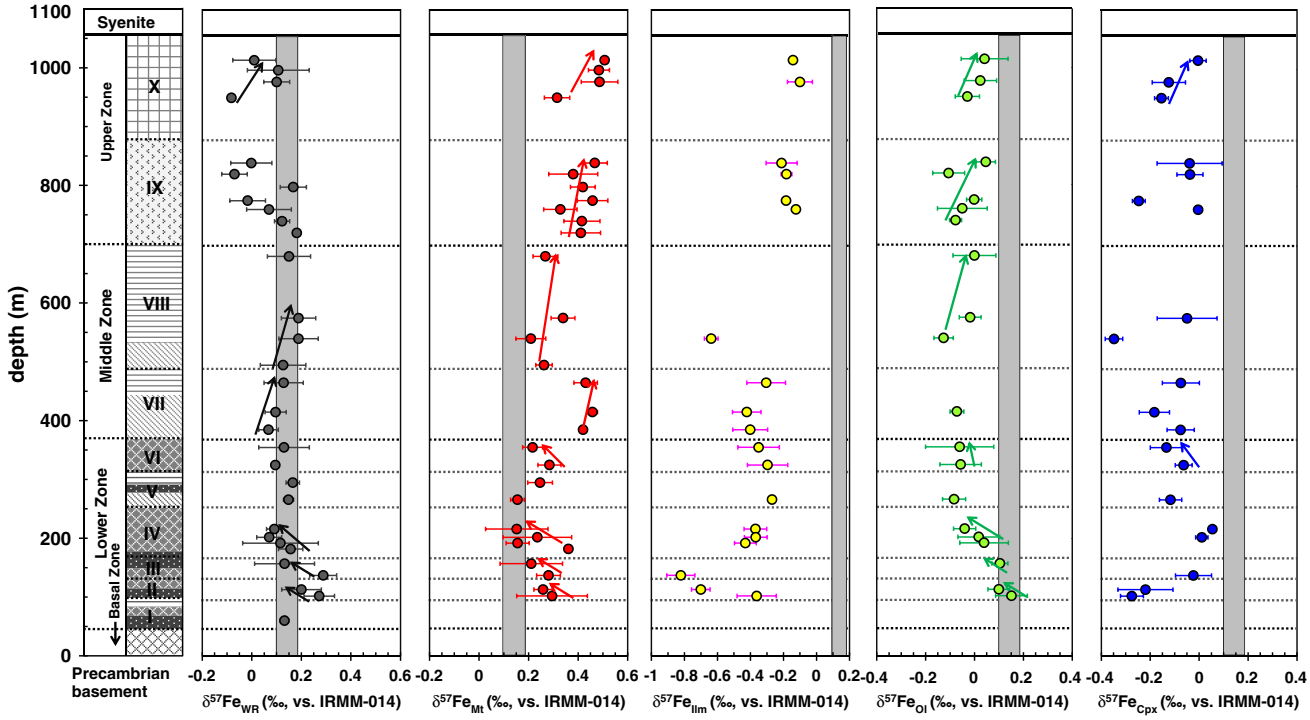

Fig. 4. Variations of $\delta^{57}Fe$ of the whole rocks (WR, relative to IRMM-014) and minerals (magnetite, ilmenite, olivine, and clinopyroxene) with relative stratigraphic position of the LZ and MZ across the Jijiping segment and the UZ across the Qinggangping segment (Fig. 2). The light gray regions ($\delta^{57}Fe = 0.10$ to 0.19‰) represent the iron isotope composition of the OIBs from Koolau and Loihi, Hawaii (Teng et al., 2013).

On the other hand, in the diagram of $\delta^{57}Fe_{Ilm}$ vs. $\delta^{57}Fe_{Ol}$ (Fig. 5e), most of the Baima samples appear above the line of $\Delta^{57}Fe_{Ilm-Ol} = 0$. The LZ and MZ samples have much lower $\Delta^{57}Fe_{Ilm-Ol}$ (−0.50 and −0.19‰) relative to the UZ samples, which have $\Delta^{57}Fe_{Ilm-Ol}$ between −0.26 and −0.07‰ (Fig. 5e). The samples with extremely low $\delta^{57}Fe_{Ilm}$ values also plot separately from the other samples (Fig. 5e).

5. Discussion

Recent studies have confirmed detectable iron isotope fractionation between olivine and melt and between magnetite and pyroxene during fractional crystallization of mafic magma (Teng et al., 2008; Sossi et al., 2012; Weyer and Seitz, 2012). However, systematic Fe isotope measurements of all the Fe-bearing minerals, including mafic-silicates and oxides, in an intrusion or a volcanic suite are still very limited. Therefore, the mechanisms and critical factors that control the Fe isotope fractionation between minerals during magma crystallization and sub-solidus re-equilibration are far from well understood. Additionally, evolution of the Fe isotope compositions of the magma and crystallizing minerals in a layered intrusion in a complex magma plumbing system are unknown. By means of the Fe isotope variations of the whole-rocks, magnetite, ilmenite, olivine, and clinopyroxene of the Baima layered intrusion, we attempt to reveal the fundamental factors governing the Fe isotope fractionation among mafic silicate minerals and Fe–Ti oxides during fractional crystallization of mafic magma and sub-solidus re-equilibration.

5.1. Inter-mineral Fe isotope fractionation during crystallization

The heavier isotopes commonly tend to incorporate in lower coordination polyhedra to form shorter (and thus stiffer) bonds in the aid of minimizing the vibrational energy associated with the bond and thus result in stable isotope fractionation, such as Fe, Mg, and Li (Polyakov and Mineev, 2000; Schauble et al., 2001; Teng et al., 2006; Liu et al., 2010, 2011; Li et al., 2011; Xiao et al., 2013). Theoretical calculations of Fe isotope equilibrium fractionation have predicted that the reduced partition function ratio (β-factor) of Fe isotope of the mineral(s) with higher $Fe^{3+}/\Sigma Fe$ is considerably greater than that of Fe^{2+}-bearing phase(s) (Polyakov and Mineev, 2000; Schauble et al., 2001; Polyakov et al., 2007). Consequently, at a given temperature, the order of β-factor of Fe isotope is: $\beta_{Mt} > \beta_{Ol,\ Cpx} > \beta_{Ilm}$ (Polyakov and Mineev, 2000). This is consistent with our observation that the magnetite is evidently richer in heavier Fe isotope than the olivine and clinopyroxene separated from the Baima rocks (Table 2, Fig. 4). Although the Baima ilmenite is higher in $Fe^{3+}/\Sigma Fe$ than the olivine and clinopyroxene (Zhang, 2013), Fe^{3+} substitutes Fe^{2+} and Ti^{4+} at octahedral sites, which have longer bonds than tetrahedral sites, and thus could not concentrate heavier isotope. Additionally, sub-solidus re-equilibration with the magnetite leads the ilmenite to become lighter in Fe isotope (see Section 5.2 below).

The fractionation factor between the minerals A and B ($\Delta^{57}Fe_{A-B}$) in equilibrium is expected to be very small at high temperature (e.g. Beard and Johnson, 2004; Williams et al., 2005; Zhao et al., 2010, 2012; Huang et al., 2011; Sossi et al., 2012). The Fe isotope equilibrium fractionation factor between phases A and B can be approximately demonstrated by the equation (Polyakov and Mineev, 2000):

$$\Delta^{57}Fe_{A\text{-}B} = \delta^{57}Fe_A\text{-}\delta^{57}Fe_B \approx C \times 10^6/T^2 \quad (1)$$

where T is the absolute temperature in K and C is the equilibrium fractionation coefficient. In the binary plot of $\delta^{57}Fe_{Ol}$ vs. $\delta^{57}Fe_{Cpx}$ (Fig. 5a), most of the Baima samples have $\Delta^{57}Fe_{Ol-Cpx}$ between −0.1‰ and +0.12‰ and plot within the area of the mantle xenoliths, in which olivine and clinopyroxene are considered to be equilibrium in Fe isotopes (Huang et al., 2011). These suggest that an approximate Fe isotope equilibrium between olivine and clinopyroxene for most of the Baima samples had been reached during fractional crystallization and preserved well during sub-solidus cooling. However, there are four samples with $\Delta^{57}Fe_{Ol-Cpx}$ larger than 0.20‰ due to very low

$\delta^{57}Fe_{Cpx}$ values, probably associated with kinetic fractionation (see Section 5.2 below).

In contrast, most of the Baima samples have the $\Delta^{57}Fe_{Mt-Ol}$ and $\Delta^{57}Fe_{Mt-Cpx}$ values larger than 0.1‰, and their $\Delta^{57}Fe_{Ilm-Ol}$ values are mostly less than −0.1‰ (Fig. 5b–e). However, the Baima LZ samples show a small range of $\Delta^{57}Fe_{Mt-Ol}$ values (+0.11 to +0.24‰, except two samples) and plot in a trend with a slope of ~1, indicating that the olivine and magnetite are roughly equilibrium in Fe isotope (Fig. 5c). According to the experiment by Shahar et al. (2008), the Fe isotope fractionation between magnetite and fayalite can be described by $\Delta^{57}Fe_{Mt-Ol} = 0.3(\pm0.024) \times 10^6/T^2$. The equilibrium fractionation coefficient (0.3 ± 0.024) is consistent with the theoretically predicted value (~0.414) according to the β-factors of magnetite by Dauphas et al. (2012, $10^3 \times \ln\beta \approx 0.984 \times 10^6/T^2$) and olivine by Polyakov and Mineev (2000, $10^3 \times \ln\beta \approx 0.570 \times 10^6/T^2$). Thus, the equilibrium fractionation coefficient is assumed to be 0.35 for the Fe isotope fractionation between the olivine and magnetite in this study and the $\Delta^{57}F_{Mt-Ol}$ equals +0.16‰ and +0.23‰ according to the Eq. (1) at 1200 and 950 °C, respectively (Fig. 5c). The temperatures are matching with the temperature range of the crystallization of the Baima intrusion predicted by Zhang et al. (2012). The $\Delta^{57}F_{Mt-Ol}$ data of most of the LZ samples match the theoretically predicted values well (Fig. 5c), indicating that the magnetite and olivine are approximately equilibrium in Fe isotope during the formation of the LZ magnetite wehrlite and magnetite troctolite and preserved principally on cooling.

A recent study of Sossi et al. (2012) indicated that the Fe isotope equilibrium fractionation between magnetite and pyroxene during crystallization of the dolerites of the Red Hill intrusion resulted in a

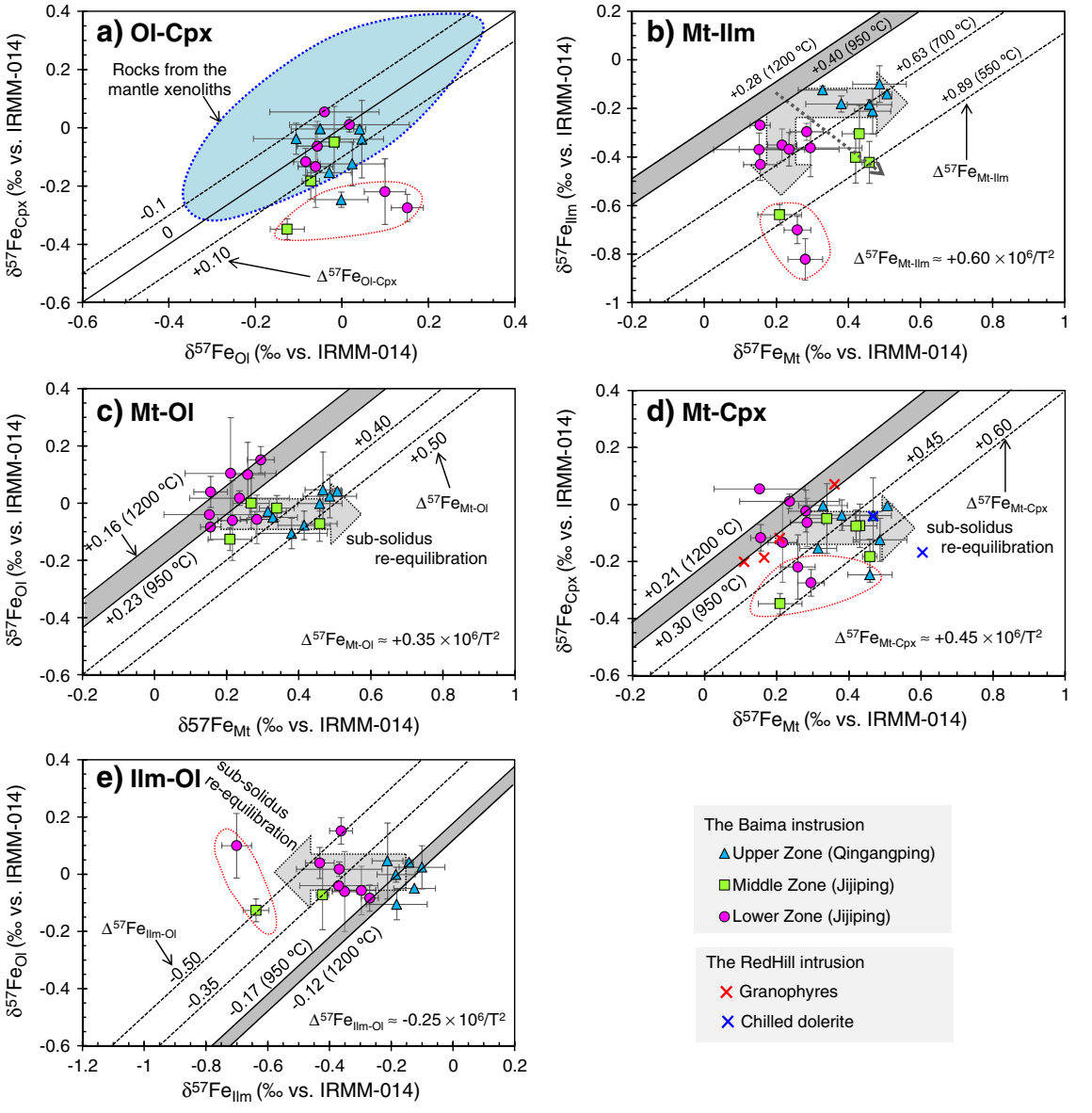

Fig. 5. Fe isotope fractionation between inter-minerals from the Baima layered intrusion. The dark gray regions are expected equilibrium Fe isotope fractionation at magmatic temperatures (~1200–950 °C, Zhang et al., 2012). The fractionation coefficient (C) between magnetite and olivine is assumed to be 0.35, which is consistent with the experimental result (Shahar et al., 2008) and the theoretical expectation of the β-factors of magnetite from Dauphas et al. (2012) and olivine from Polyakov and Mineev (2000). The C between magnetite and clinopyroxene is assumed to be 0.45, which is derived from the study of the Red Hill intrusion (Sossi et al., 2012). The C between magnetite and ilmenite is set to be 0.60, which is resulted from the theoretical calculation of the magnetite β-factor from Dauphas et al. (2012) and ilmenite β-factor from Polyakov and Mineev (2000). The light gray arrows represent the trends of Fe isotopic variations of magnetite (and ilmenite) modified by sub-solidus re-equilibration. A few of clinopyroxene and ilmenite within the fields of red point line are clearly lighter in $\delta^{57}Fe$ values and may be related to kinetic isotope fractionation. The light blue area in plot (a) represents the $\delta^{57}Fe$ of most mantle xenoliths olivine and clinopyroxene from Zhu et al. (2002), Beard and Johnson (2004), Williams et al. (2005), Weyer and Ionov (2007), Zhao et al. (2010, 2012) and Huang et al. (2011). Six clinopyroxene–magnetite pairs of the Red Hill intrusion in plot (d) are from Sossi et al. (2012).

positive correlation between $\delta^{57}Fe_{Mt}$ and $\delta^{57}Fe_{Cpx}$, whereas the decrease of $\delta^{57}Fe_{Cpx}$ and elevation of $\delta^{57}Fe_{Mt}$ in the marginal rocks were attributed to kinetic fractionation (Fig. 5d). Most of the LZ samples (except for the samples SB09-11 and -13 with very low $\delta^{57}Fe_{Cpx}$) plot together with the dolerites of the Red Hill intrusion, suggesting that the Fe isotope equilibrium between magnetite and clinopyroxene reached during crystallization was roughly preserved (Fig. 5d). The $\Delta^{57}F_{Mt-Cpx}$ of most of the LZ samples are also roughly matching with the theoretically calculated $\Delta^{57}F_{Mt-Cpx}$ values (~0.21 to 0.30‰) within analytical errors at temperatures of 1200 and 950 °C, respectively (Fig. 5d), if the equation of $\Delta^{57}F_{Mt-Cpx} \approx 0.45 \times 10^6/T^2$ is approximately applicable according to Sossi et al. (2012). This equation is well confirmed with the theoretical β-factors of magnetite and clinopyroxene ($10^3 \times \ln\beta \approx 0.984 \times 10^6/T^2$ and $10^3 \times \ln\beta \approx 0.484 \times 10^6/T^2$, respectively) proposed by Dauphas et al. (2012) and by Polyakov and Mineev (2000).

The above observations suggest that Fe isotope equilibrium between magnetite and olivine and clinopyroxene was achieved during crystallization and preserved in sub-solidus cooling for most of the LZ samples. However, progressively heavier $\delta^{57}Fe_{Mt}$ and higher $\Delta^{57}Fe_{Mt-Ol}$ and $\Delta^{57}Fe_{Mt-Cpx}$ of the MZ and UZ samples than those of the LZ samples imply a re-equilibration below 950 °C (Fig. 5c, d; see Section 5.2 below).

In the diagram of $\delta^{57}Fe_{Ilm}$ vs. $\delta^{57}Fe_{Ol}$, the UZ samples plot near the lines showing Fe isotope equilibration between ilmenite and olivine predicted by the theoretical equations of $\Delta^{57}Fe_{Ilm-Ol} \approx -0.25 \times 10^6/T^2$ proposed by Polyakov and Mineev (2000) under 1200 and 950 °C (Fig. 5e). However, the low $\delta^{57}Fe$ values of the LZ and MZ ilmenite reflect a clear re-equilibration below 950 °C (Fig. 5e; see Section 5.2 below).

5.2. Sub-solidus Fe isotope re-equilibration

The agreements between the $\delta^{57}Fe$ data of the LZ magnetite and olivine and clinopyroxene and the theoretically predicted values of $\Delta^{57}Fe_{Mt-Ol}$ and $\Delta^{57}Fe_{Mt-Cpx}$ indicate that the Fe isotope equilibrations among these minerals reached during crystallization are preserved well (Fig. 5c, d). However, the $\Delta^{57}Fe_{Mt-Ilm}$ values of the Baima rocks (0.42 to 0.88‰, with except for three samples) are evidently larger than the theoretical predictions (0.27 to 0.39‰) by the equation $\Delta^{57}Fe_{Mt-Ilm} \approx 0.60 \times 10^6/T^2$ according to the β-factors of magnetite of Dauphas et al. (2012) and ilmenite of Polyakov and Mineev (2000) under temperatures of 1200 to 950 °C (Fig. 5b). This clearly indicates that the correlations of the Fe isotopic compositions between the magnetite and the ilmenite of the Baima intrusion do not reflect the Fe isotope equilibrium during crystallization at high temperatures. Instead, such discrepancies are most likely resulted from sub-solidus re-equilibration between the magnetite and the ilmenite on cooling. However, some questions are inevitable: (1) whether or not sub-solidus re-equilibration in Fe isotope really occurs between magnetite and ilmenite? and (2) can the Fe isotope equilibration reached during crystallization between the magnetite and silicate minerals be preserved?

The sub-solidus chemical re-equilibration between magnetite and ilmenite can be achieved via the reaction of Fe_2TiO_4 (in Mt) + Fe_2O_3 (in Ilm) = $FeTiO_3$ (in Ilm) + Fe_3O_4 (in Mt), which proceeds to the right as temperature decreasing and engenders the Fe–Ti oxides to be purer in compositions (Frost and Lindsley, 1991). Such sub-solidus reaction is common in the Baima intrusion because magnetite and ilmenite always occur together in the rocks, even in the samples having low contents of oxides (Fig. 2). Theoretical studies of Fe isotope fractionation indicate that heavy Fe isotopes tend to concentrate the phases in which Fe^{3+} is the predominate cation and are more preferential to occupy the sites of IV-fold coordination than VI-fold coordination in a mineral (Schauble et al., 2001). In magnetite, half of Fe^{3+} situates at IV-fold coordination, and Fe^{2+} and another half of Fe^{3+} situate at VI-fold coordination. Whereas, both Fe^{2+} and Fe^{3+}, which substitute for Ti^{4+}, occupy VI-fold coordination in ilmenite (Deer et al., 1996). Thus, it is predictable that magnetite will become significantly heavier in Fe isotope composition than ilmenite through the sub-solidus re-equilibration reaction. Using the QUILF program of Andersen et al. (1993), Pang et al. (2008b) estimated the magnetite–ilmenite sub-solidus re-equilibration in the Panzhihua intrusion that occurred until temperatures decreased to 550 °C. The geochronology, petrology and mineralogy similarities between the Baima and Panzhihua intrusions and their genetic linkage with the Emeishan mantle plume (Zhou et al., 2002; Zhang et al., 2012; Song et al., 2013) permit us to propose that the sub-solidus re-equilibration between magnetite and ilmenite also occurred in the Baima intrusion. This is supported by the well-developed exsolution ilmenite lamellae in the magnetite of the Baima intrusion (Zhang et al., 2012). Thus, we propose that the sub-solidus re-equilibration in Fe isotopes between the magnetite and ilmenite was resulted from the reaction of Fe_2TiO_4 (in Mt) + Fe_2O_3 (in Ilm) = $FeTiO_3$ (in Ilm) + Fe_3O_4 (in Mt).

On the other hand, the Fe isotopic variations of the magnetite and ilmenite during the sub-solidus re-equilibration would also be strongly controlled by the proportions of the two minerals in the rocks in mass balance consideration. As mentioned above, the ratios of magnetite/ilmenite are as high as 5.8–10.3 in the LZ magnetite wehrlite and troctolite and are as low as 1.1–3.7 in the UZ apatite gabbro (Figs. 1, 2). Therefore, although the sub-solidus re-equilibration caused obvious decrease of the $\delta^{57}Fe_{Ilm}$ in the LZ rocks, the $\delta^{57}Fe_{Mt}$ varied a little owing to much more magnetite than ilmenite in the rocks (Fig. 5b). In contrast, the $\delta^{57}Fe$ values of the UZ magnetite increased evidently because of the re-equilibration between the magnetite and ilmenite, while the $\delta^{57}Fe_{Ilm}$ values had a relatively small variation because of low magnetite/ilmenite ratios (Fig. 5b). This is the probable reason that the magnetite remains nearly equilibrium with olivine and clinopyroxene in Fe isotope in most of the LZ samples (Fig. 5c, d), whereas the ilmenite displays roughly equilibrium with olivine in the UZ rocks (Fig. 5e). On the other hand, both magnetite and ilmenite of the MZ rocks have prominent variations in their Fe isotopic compositions because of the moderate magnetite/ilmenite ratios (Figs. 1, 2, 5b). Particularly, the rocks of the cyclic unit VII show the extremely high $\delta^{57}Fe_{Mt}$ and very low $\delta^{57}F_{Ilm}$ values (Fig. 4).

Oxide-silicate re-equilibration is marked by limited Fe^{2+}–Mg^{2+} exchange between Fe–Ti oxides and mafic silicates (Frost et al., 1988; Frost and Lindsley, 1991). These exchange reactions result in the oxides tending to lose Mg^{2+} to co-existing silicates and extract Fe^{2+} from them. However, such Fe^{2+}–Mg^{2+} exchange could only lead to minor decrease of $\delta^{57}Fe$ of the Fe–Ti oxides because only a small amount of Fe^{3+} is involved in the reaction. Additionally, the blocking temperature of the oxide-silicate sub-solidus reaction in the Baima intrusion should

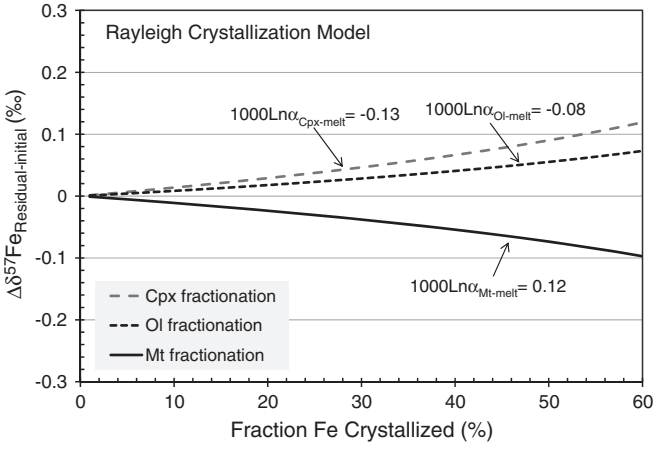

Fig. 6. Rayleigh fractionation model ($\delta^{57}Fe_{residual}/\delta^{57}Fe_{initial} = f^{\alpha-1}$) for Fe isotope fractionation during magmatic differentiation. The isotope fractionation coefficients between magnetite, clinopyroxene and silicate melt are from Sossi et al. (2012), and the coefficient between olivine and silicate melt is based on Teng et al. (2008).

be similar to that in the Panzhihua intrusion, which was estimated to be above ~950 °C (Pang et al., 2008b). Therefore, it is difficult to attribute the Fe isotope discrepancies appearing in the diagrams of magnetite and ilmenite vs. olivine and clinopyroxene to the oxide-silicate re-equilibration (Fig. 5c–e).

It is noticed that a few of samples (SB09-11 and -13 of the LZ, SB09-32 of the MZ and SB11-57 of the UZ) display anomalous depletion in $\delta^{57}Fe_{Cpx}$ and $\delta^{57}Fe_{Ilm}$ (Table 2, Fig. 5). Such δ^{57}Fe-depletions of the clinopyroxene and ilmenite cannot be explained by Fe isotope equilibrium fractionation during crystallization or sub-solid re-equilibration, but may be attributed to kinetic isotope fractionation. Kinetic Fe isotope fractionation have been observed in natural and experimental systems recently (Dauphas, 2007; Teng et al., 2008, 2011; Richter et al., 2009a, b; Huang et al., 2011; Sossi et al., 2012), although the mechanism is still unclear. Roskosz et al. (2006) and Richter et al. (2009a) proposed that chemical diffusion can promote isotopic fractionation between two phases, owing to the faster diffusivity of the lighter isotope than the heavier one during magma crystallization. The significant heterogeneities in Fe isotope of magnetite and ilmenite from IODP Hole 1256D (eastern equatorial Pacific) were originated from kinetic fractionation effects, caused by the interaction of magnetite/ilmenite with hydrothermal fluids and/or incomplete re-equilibration at low temperatures (Dziony et al., 2014). Kinetic isotope fractionation resulted in anomalously large variation in δ^{57}Fe of the olivine phenocrysts (+0.1 to −1.7‰) with relatively small chemical variation (Fo_{80} to Fo_{84}) in a single sample of the Hawaiian basalts (Teng et al., 2008, 2011). However, in the Baima intrusion, although the olivine has a large compositional variation (Fo_{55} to Fo_{74}, Zhang et al., 2012), the small range of $\delta^{57}Fe_{Ol}$ values (−0.15 to +0.15‰) implies no kinetic isotope fractionation for the olivine.

5.3. Petrogenesis implications

Both olivine and pyroxene incorporate ferrous iron (McCanta et al., 2004; Mallmann and O'Neill, 2009) and thus preferentially extract the lighter Fe isotope as opposed to the magma at equilibrium (Polyakov and Mineev, 2000). Thus, fractional crystallization of olivine and pyroxene will result in enrichment of heavy Fe isotope in the residual magma (Fig. 6). Consistently, fractional crystallization of olivine leads to elevation of δ^{57}Fe with decreasing MgO of the Kilauea Iki lava at Hawaii (Teng et al., 2008). On the other hand, fractional crystallization of magnetite will lead to the residual magma depleted in heavy Fe isotope (Fig. 6).

The higher δ^{57}Fe values (0.10 to 0.15‰, Table 2, Fig. 4) and lower Fo percentages (66–74, Fig. 1) of the olivine of the cyclic units II and III than the olivine phenocrysts in the Hawaii Kilauea Iki Lava Lake basalt (<0.10‰ and 67–80.2, respectively, Teng et al., 2008) indicate that the parental magma of the Baima LZ is more differentiated. According to the equation ($\Delta^{57}Fe_{Ol-Melt} \approx -0.15 \times 10^6/T^2$) proposed by Teng et al. (2008) and assuming the olivine crystallized at ~1150 °C (Zhang et al., 2012), the δ^{57}Fe value of the parental magma equilibrium with the olivine should be ~0.16–0.20‰. This means that the parental magma are slightly heavier in Fe isotope than the MORB (δ^{57}Fe = ~0.15‰ in average, see Teng et al., 2013 and references therein). This is consistent with the conclusion that the parental magmas of the Baima intrusion were generated by extensive fractional crystallization of olivine and pyroxene of a high-Ti picritic magma in a deep-seated magma chamber proposed by Zhang et al. (2012). Such fractionation at depth led to the enrichment of not only Fe–Ti but also heavy Fe isotope in the evolved magma. Similarly, Teng et al. (2013) recently proposed that fractional crystallization of mafic-silicates can give rise to elevation of δ^{57}Fe values in the magma up to ~0.24‰ and Fe isotopic heterogeneities of the OIBs from Koolau and Loihi in Hawaii and the Society Islands and Cook-Austral chain in French Polynesia.

Above descriptions have indicated that the most conspicuous feature of the LZ is that the values of $\delta^{57}Fe_{Ol}$ and the $\delta^{57}Fe_{Mt}$ decrease regularly from the base upward in most of the cyclic units (Table 2, Fig. 4). This is concordant with the extensively early crystallization and accumulation of the Fe–Ti oxides along with silicates from the replenished Fe–Ti-enriched magmas and the formation of the stratiform Fe–Ti

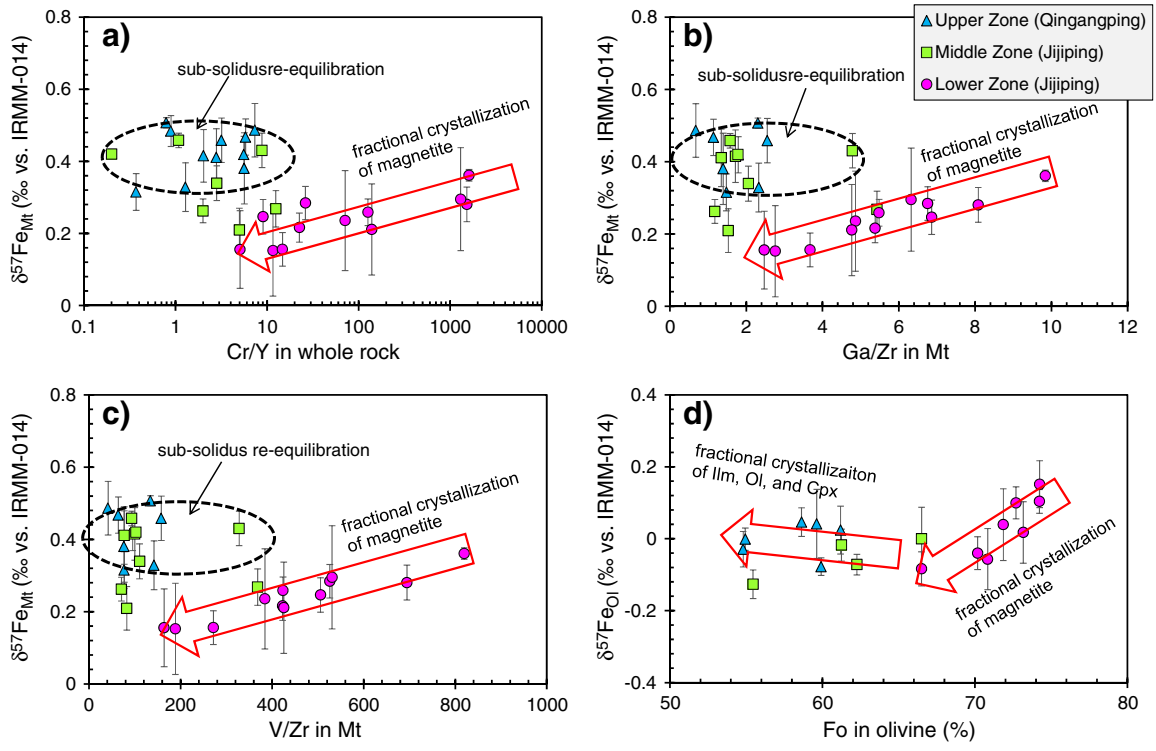

Fig. 7. Variations of $\delta^{57}Fe_{Mt}$ vs. Cr/Y ratios in whole rocks (a), V/Zr and Ga/Zr ratios in magnetite (b and c, respectively), and $\delta^{57}Fe_{Ol}$ vs. forsterite percentages of olivine (d). Cr/Y ratios of whole rock and Fo contents in olivine are after Zhang et al. (2012), and V, Ga and Zr contents of magnetite are from our unpublished data.

oxide ore layers in the lower half of the cyclic units of the LZ (Fig. 1, Zhang et al., 2012). The partition coefficient of Cr between magnetite and basaltic magma $D_{Cr}^{Mt/melt}$ (=153, Schock, 1979) is much higher than $D_{Cr}^{Cpx/melt}$ (=3.8, Hart and Dunn, 1993) and $D_{Cr}^{Ol/melt}$ (=0.73, Nikogosian and Sobolev, 1997). Vanadium and Ga are compatible to magnetite ($D_{V}^{Mt/melt}$ = 26, $D_{Ga}^{Mt/melt}$ = 2) but are incompatible to silicate minerals (Paster et al., 1974; Duke, 1976; Villemant et al., 1981). However, Y and Zr are incompatible for both the Fe–Ti oxides and silicate minerals (McCallum and Charette, 1978; Nielsen et al., 1992; Hart and Dunn, 1993). Thus, both the Cr/Y ratio of the cumulus rocks and the V/Zr and Ga/Zr ratios of the magnetite will decrease during the fractional crystallization of magnetite. Although crystallization of silicates and ilmenite could cause the residual magma slightly heavier in Fe isotope, extensive fractional crystallization of magnetite will result in obvious δ^{57}Fe-depletion in the residual magma. The Fe isotope fractionation owing to the extensive fractional crystallization of the magnetite can be testified by the concurrent $\delta^{57}Fe_{Mt}$ depletion along with the decreases of the whole-rock Cr/Y ratios and the V/Zr and Ga/Zr ratios of the magnetite in the LZ, respectively (Fig. 7a–c). The evidently positive correlation between $\delta^{57}Fe_{Ol}$ and Fo of olivine in the LZ again reveals the extraction of heavy Fe isotope by the early crystallizing magnetite (Fig. 7d). In contrast, the MZ and UZ magnetite had been enriched in δ^{57}Fe due to the sub-solidus re-equilibration with the ilmenite in Fe isotope although they have low Ga/Zr and V/Zr ratios (Fig. 7b, c).

The interstitial and anhedral features clearly demonstrate that the Fe–Ti oxides in the Baima MZ and UZ rocks crystallized later than the silicates (Fig. 2a–b; Zhang et al., 2012). Thus, an elevation of the heavy Fe isotope in the magma is predictable depending on the intensity of the fractional crystallization of the olivine and clinopyroxene. The gradual enrichment of heavy Fe isotope in the evolved magma is recorded by the limited data and displays a weak increase of the $\delta^{57}Fe_{Ol}$ values upwards in the cyclic units VIII, IX and X (Fig. 4), because olivine remains the Fe isotope equilibrium with the magma as demonstrated above. The slightly negative correlations between the $\delta^{57}Fe_{Ol}$ and Fo values of the MZ and UZ olivine also illustrate that the Fe isotope composition of the evolved magma became heavier due to segregation of crystallized olivine and clinopyroxene (Fig. 7d).

6. Conclusions

Fractional crystallization can result in Fe isotope fractionation between Fe-bearing minerals in mafic–ultramafic intrusion. The Fe isotope fractionation between minerals is controlled by mineral composition and structure because heavier Fe isotopes tend to incorporate in lower co-ordination polyhedra and form shorter bonds. For most of the Baima samples, the δ^{57}Fe values systematically decrease from magnetite, to olivine and/or clinopyroxene, then to ilmenite. Extensive early fractional crystallization and accumulation of the magnetite resulted in the regular decrease in δ^{57}Fe values of the magnetite and olivine from the base upward in most of the cyclic units in the Lower Zone. In contrast, the slight elevation of $\delta^{57}Fe_{Ol}$ values upwards in the cyclic units of the Middle and Upper zones was attributed to early crystallization of olivine and clinopyroxene. The reversals in $\delta^{57}Fe_{Mt}$ and $\delta^{57}Fe_{Ol}$ values suggest multiple recharges of magma.

Olivine and clinopyroxene can preserve their original Fe isotopic values well relative to the oxides in sub-solidus re-equilibration. However, sub-solidus exchange of Fe^{3+} versus Fe^{2+} and T^{4+} between magnetite and ilmenite can result in elevation of $\delta^{57}Fe_{Mt}$ and decrease of $\delta^{57}F_{Ilm}$. Furthermore, the sub-solidus re-equilibration of Fe isotope is also controlled by the proportions between the two oxides. Thus, the sub-solidus Fe isotope re-equilibration caused obviously minor variation of $\delta^{57}Fe_{Mt}$ and decrease of $\delta^{57}F_{Ilm}$ in the Lower Zone because of the high magnetite/ilmenite ratios, whereas both $\delta^{57}Fe_{Mt}$ and $\delta^{57}F_{Ilm}$ have been evidently modified by sub-solidus re-equilibration in the Middle Zone owing to the moderate magnetite/ilmenite ratios.

Acknowledgments

This study is supported by the National Basic Research Program of China (2012CB416804, 2012CB416806), the CAS/SAFEA International Partnership Program for Creative Research Teams — (Intraplate Mineralization Research Team; KZZD-EW-TZ-20), the Research Fund from SKLODG (SKLODG-ZY125-06, 201201) and NSFC research grants (41172090, 41373042, and 41103002). We greatly appreciate two anonymous reviewers for their constructive reviews that have greatly improved this manuscript and Professor David Hilton for efficient editorial handling. Many thanks are due to Drs. A.-G. Dong, J. Sun, Z.-H. Li, and J. Li for their kind help on the analysis of Fe isotope and Mr. J.-F. Zhang and S.-G. Gui for their assistance during the fieldwork.

References

Ali, J.R., Thompson, G.M., Zhou, M.-F., Song, X., 2005. Emeishan large igneous province, SW China. Lithos 79 (3–4), 475–489.
Andersen, D.J., Lindsley, D.H., Davidson, P.M., 1993. QUILF: a pascal program to assess equilibria among Fe–Mg–Mn–Ti oxides, pyroxenes, olivine, and quartz. Comput. Geosci. 19 (9), 1333–1350.
Bai, Z.-J., Zhong, H., Naldrett, A.J., Zhu, W.-G., Xu, G.-W., 2012. Whole-rock and mineral composition constraints on the genesis of the giant Hongge Fe–Ti–V oxide deposit in the Emeishan Large Igneous Province, Southwest China. Econ. Geol. 107 (3), 507–524.
Beard, B.L., Johnson, C.M., 1999. High precision iron isotope measurements of terrestrial and lunar materials. Geochim. Cosmochim. Acta 63 (11–12), 1653–1660.
Beard, B.L., Johnson, C.M., Skulan, J.L., Nealson, K.H., Cox, L., Sun, H., 2003. Application of Fe isotopes to tracing the geochemical and biological cycling of Fe. Chem. Geol. 195 (1–4), 87–117.
Beard, B.L., Johnson, C.M., 2004. Inter-mineral Fe isotope variations in mantle-derived rocks and implications for the Fe geochemical cycle. Geochim. Cosmochim. Act. 68 (22), 4727–4743.
Chung, S.L., Jahn, B.M., 1995. Plume-lithosphere interaction in generation of the Emeishan flood basalts at the Permian–Triassic boundary. Geology 23 (10), 889–892.
Craddock, P.R., Dauphas, N., 2011. Iron isotopic compositions of geological reference materials and chondrites. Geostand. Geoanal. Re. 35 (1), 101–123.
Dauphas, N., 2007. Diffusion-driven kinetic isotope effect of Fe and Ni during formation of the Widmanstätten pattern. Meteorit. Planet. Sci. 42 (9), 1597–1613.
Dauphas, N., Janney, P.E., Mendybaev, R.A., Wadhwa, M., Richter, F.M., Davis, A.M., van Zuilen, M., Hines, R., Foley, C.N., 2004. Chromatographic separation and multicollection-ICPMS analysis of iron. investigating mass-dependent and -independent isotope effects. Anal. Chem. 76 (19), 5855–5863.
Dauphas, N., Craddock, P.R., Asimow, P.D., Bennett, V.C., Nutman, A.P., Ohnenstetter, D., 2009. Iron isotopes may reveal the redox conditions of mantle melting from Archean to Present. Earth Planet. Sci. Lett. 288 (1–2), 255–267.
Dauphas, N., Roskosz, M., Alp, E.E., Golden, D.C., Sio, C.K., Tissot, F.L.H., Hu, M.Y., Zhao, J., Gao, L., Morris, R.V., 2012. A general moment NRIXS approach to the determination of equilibrium Fe isotopic fractionation factors: application to goethite and jarosite. Geochim. Cosmochim. Acta 94, 254–275.
Deer, W.A., Howie, R.A., Zussman, J., 1996. An Introduction to the Rock-forming Minerals, 2nd edition. Prentice Hall.
Duke, J.M., 1976. Distribution of the period four transition elements among olivine, calcic clinopyroxene and mafic silicate liquid: experimental results. J. Petrol. 17 (4), 499–521.
Dziony, W., Horn, I., Lattard, D., Koepke, J., Steinhoefel, G., Schuessler, J.A., Holtz, F., 2014. In-situ Fe isotope ratio determination in Fe–Ti oxides and sulfides from drilled gabbros and basalt from the IODP Hole 1256D in the eastern equatorial Pacific. Chem. Geol. 363, 101–113.
Frost, B.R., Lindsley, D.H., 1991. Occurrence of iron–titanium oxides in igneous rocks. Rev. Mineral. Geochem. 25 (1), 433–468.
Frost, B.R., Lindsley, D.H., Andersen, D.J., 1988. Fe–Ti oxide–silicate equilibria; assemblages with fayalitic olivine. Am. Mineral. 73 (7–8), 727–740.
Hart, S., Dunn, T., 1993. Experimental cpx/melt partitioning of 24 trace elements. Contrib. Mineral. Petrol. 113 (1), 1–8.
Howarth, G.H., Prevec, S.A., Zhou, M.-F., 2013. Timing of Ti-magnetite crystallisation and silicate disequilibrium in the Panzhihua mafic layered intrusion: implications for ore-forming processes. Lithos 170–171, 73–89.
Huang, F., Zhang, Z.F., Lundstrom, C.C., Zhi, X.C., 2011. Iron and magnesium isotopic compositions of peridotite xenoliths from Eastern China. Geochim. Cosmochim. Act. 75 (12), 3318–3334.
Li, W.-Y., Teng, F.-Z., Xiao, Y., Huang, J., 2011. High-temperature inter-mineral magnesium isotope fractionation in eclogite from the Dabie orogen, China. Earth Planet. Sci. Lett. 304 (1–2), 224–230.
Liu, S.-A., Teng, F.-Z., He, Y., Ke, S., Li, S., 2010. Investigation of magnesium isotope fractionation during granite differentiation: implication for Mg isotopic composition of the continental crust. Earth Planet. Sci. Lett. 297 (3–4), 646–654.
Liu, S.-A., Teng, F.-Z., Yang, W., Wu, F.-Y., 2011. High-temperature inter-mineral magnesium isotope fractionation in mantle xenoliths from the North China craton. Earth Planet. Sci. Lett. 308 (1–2), 131–140.

Luan, Y., Song, X.-Y., Chen, L.-M., Zheng, W.-Q., Zhang, X.-Q., Yu, S.-Y., She, Y.-W., Tian, X.-L., Ran, Q.-Y., 2014. Key factors controlling the accumulation of the Fe–Ti oxides in the Hongge layered intrusion in the Emeishan Large Igneous Province, SW China. Ore Geol. Rev. 57, 518–538.
Mallmann, G., O'Neill, H.S.C., 2009. The crystal/melt partitioning of V during mantle melting as a function of oxygen fugacity compared with some other elements (Al, P, Ca, Sc, Ti, Cr, Fe, Ga, Y, Zr and Nb). J. Petrol. 50 (9), 1765–1794.
McCallum, I.S., Charette, M.P., 1978. Zr and Nb partition coefficients: implications for the genesis of mare basalts, KREEP and sea floor basalts. Geochim. Cosmochim. Acta 42 (6), 859–869.
McCanta, M.C., Dyar, M.D., Rutherford, M.J., Delaney, J.S., 2004. Iron partitioning between basaltic melts and clinopyroxene as a function of oxygen fugacity. Am. Mineral. 89 (11–12), 1685–1693.
Nielsen, R., Gallahan, W., Newberger, F., 1992. Experimentally determined mineral-melt partition coefficients for Sc, Y and REE for olivine, orthopyroxene, pigeonite, magnetite and ilmenite. Contrib. Mineral. Petrol. 110 (4), 488–499.
Nikogosian, I.K., Sobolev, A.V., 1997. Ion-microprobe analysis of melt inclusions in olivine: experience in estimating the olivine-melt partition coefficients of trace elements. Geochem. Int. 35 (2), 119–126.
Pang, K.N., Li, C.S., Zhou, M.F., Ripley, E.M., 2008a. Abundant Fe–Ti oxide inclusions in olivine from the Panzhihua and Hongge layered intrusions, SW China: evidence for early saturation of Fe–Ti oxides in ferrobasaltic magma. Contrib. Mineral. Petrol. 156 (3), 307–321.
Pang, K.N., Zhou, M.F., Lindsley, D., Zhao, D., Malpas, J., 2008b. Origin of Fe–Ti oxide ores in mafic intrusions: evidence from the Panzhihua intrusion, SW China. J. Petrol. 49 (2), 295–313.
Panxi Geological Unit, 1984. Mineralization and exploration forecasting of V-Ti magnetite deposits in the Panzhihua-Xichang region. Unpublished.
Paster, T.P., Schauwecker, D.S., Haskin, L.A., 1974. The behavior of some trace elements during solidification of the Skaergaard layered series. Geochim. Cosmochim. Acta 38 (10), 1549–1577.
Poitrasson, F., Delpech, G., Grégoire, M., 2013. On the iron isotope heterogeneity of lithospheric mantle xenoliths: implications for mantle metasomatism, the origin of basalts and the iron isotope composition of the Earth. Contrib. Mineral. Petrol. 165 (6), 1243–1258.
Polyakov, V.B., Mineev, S.D., 2000. The use of Mössbauer spectroscopy in stable isotope geochemistry. Geochim. Cosmochim. Acta 64 (5), 849–865.
Polyakov, V.B., Clayton, R.N., Horita, J., Mineev, S.D., 2007. Equilibrium iron isotope fractionation factors of minerals: reevaluation from the data of nuclear inelastic resonant X-ray scattering and Mössbauer spectroscopy. Geochim. Cosmochim. Act. 71 (15), 3833–3846.
Richter, F.M., Dauphas, N., Teng, F.-Z., 2009a. Non-traditional fractionation of non-traditional isotopes: evaporation, chemical diffusion and Soret diffusion. Chem. Geol. 258 (1–2), 92–103.
Richter, F.M., Watson, E.B., Mendybaev, R., Dauphas, N., Georg, B., Watkins, J., Valley, J., 2009b. Isotopic fractionation of the major elements of molten basalt by chemical and thermal diffusion. Geochim. Cosmochim. Acta 73 (14), 4250–4263.
Roskosz, M., Luais, B., Watson, H.C., Toplis, M.J., Alexander, C.M.O.D., Mysen, B.O., 2006. Experimental quantification of the fractionation of Fe isotopes during metal segregation from a silicate melt. Earth Planet. Sci. Lett. 248 (3–4), 851–867.
Schauble, E.A., Rossman, G.R., Taylor Jr., H.P., 2001. Theoretical estimates of equilibrium Fe-isotope fractionations from vibrational spectroscopy. Geochim. Cosmochim. Acta 65 (15), 2487–2497.
Schock, H.H., 1979. Distribution of rare-earth and other trace elements in magnetites. Chem. Geol. 26 (1–2), 119–133.
Schoenberg, R., Marks, M.A.W., Schuessler, J.A., von Blanckenburg, F., Markl, G., 2009. Fe isotope systematics of coexisting amphibole and pyroxene in the alkaline igneous rock suite of the Ilímaussaq Complex, South Greenland. Chem. Geol. 258 (1–2), 65–77.
Schuessler, J.A., Schoenberg, R., Sigmarsson, O., 2009. Iron and lithium isotope systematics of the Hekla volcano, Iceland—Evidence for Fe isotope fractionation during magma differentiation. Chem. Geol. 258 (1–2), 78–91.
Shahar, A., Young, E.D., Manning, C.E., 2008. Equilibrium high-temperature Fe isotope fractionation between fayalite and magnetite: an experimental calibration. Earth Planet. Sci. Lett. 268 (3–4), 330–338.
She, Y.-W., Yu, S.-Y., Song, X.-Y., Chen, L.-M., Zheng, W.-Q., Luan, Y., 2014. The formation of P-rich Fe–Ti oxide ore layers in the Taihe layered intrusion, SW China: implications for magma-plumbing system process. Ore Geol. Rev. 57, 539–559.
Shellnutt, J.G., Denyszyn, S.W., Mundil, R., 2012. Precise age determination of mafic and felsic intrusive rocks from the Permian Emeishan large igneous province (SW China). Gondwana Res. 22 (1), 118–126.
Song, X.-Y., Zhou, M.-F., Hou, Z.-Q., Cao, Z.-M., Wang, Y.-L., Li, Y.-G., 2001. Geochemical constraints on the mantle source of the upper permian Emeishan continental flood basalts, southwestern China. Int. Geol. Rev. 43 (3), 213–225.
Song, X.-Y., Zhou, M.-F., Cao, Z.-M., Robinson, P.T., 2004. Late permian rifting of the South China Craton caused by the Emeishan mantle plume? J. Geol. Soc. 161, 773–781.
Song, X.-Y., Qi, H.-W., Robinson, P.T., Zhou, M.-F., Cao, Z.-M., Chen, L.-M., 2008. Melting of the subcontinental lithospheric mantle by the Emeishan mantle plume; evidence from the basal alkaline basalts in Dongchuan, Yunnan, Southwestern China. Lithos 100 (1–4), 93–111.
Song, X.-Y., Keays, R.R., Xiao, L., Qi, H.-W., Ihlenfeld, C., 2009. Platinum-group element geochemistry of the continental flood basalts in the central Emeisihan Large Igneous Province, SW China. Chem. Geol. 262 (3–4), 246–261.
Song, X.-Y., Qi, H.-W., Hu, R.-Z., Chen, L.-M., Yu, S.-Y., Zhang, J.-F., 2013. Formation of thick stratiform Fe–Ti oxide layers in layered intrusion and frequent replenishment of fractionated mafic magma: evidence from the Panzhihua intrusion, SW China. Geochem. Geophys. Geosyst. 14 (3), 712–732.
Sossi, P., Foden, J., Halverson, G., 2012. Redox-controlled iron isotope fractionation during magmatic differentiation: an example from the Red Hill intrusion, S. Tasmania. Contrib. Mineral. Petrol. 164 (5), 757–772.
Tang, S.-H., Yan, B., Zhu, X.-K., Li, J., Li, S.-Z., 2012. Iron, copper and zinc isotopic compositions of basaltic standard reference material. Rock Miner. Anal. 31 (2), 218–224 (in Chinese with English abstract).
Teng, F.-Z., McDonough, W.F., Rudnick, R.L., Walker, R.J., Sirbescu, M.-L.C., 2006. Lithium isotopic systematics of granites and pegmatites from the Black Hills, South Dakota. Am. Mineral. 91 (10), 1488–1498.
Teng, F.-Z., Dauphas, N., Helz, R.T., 2008. Iron isotope fractionation during magmatic differentiation in Kilauea Iki Lava Lake. Science 320 (5883), 1620–1622.
Teng, F.-Z., Dauphas, N., Helz, R.T., Gao, S., Huang, S., 2011. Diffusion-driven magnesium and iron isotope fractionation in Hawaiian olivine. Earth Planet. Sci. Lett. 308 (3–4), 317–324.
Teng, F.-Z., Dauphas, N., Huang, S., Marty, B., 2013. Iron isotopic systematics of oceanic basalts. Geochim. Cosmochim. Acta 107, 12–26.
Urey, H.C., 1947. The thermodynamic properties of isotopic substances. J. Chem. Soc. 562–581 (Resumed).
Villemant, B., Jaffrezic, H., Joron, J.-L., Treuil, M., 1981. Distribution coefficients of major and trace elements; fractional crystallization in the alkali basalt series of Chaîne des Puys (Massif Central, France). Geochim. Cosmochim. Acta 45 (11), 1997–2016.
Wang, S.-X., 2013. Iron Isotope Geochemistry of Magmatic Evolution. Institute of Geology, Chinese Academy of Geological Sciences, Beijing.
Wang, Y., Zhu, X.-K., Mao, J.-W., Li, Z.-H., Cheng, Y.-B., 2011. Iron isotope fractionation during skarn-type metallogeny: a case study of Xinqiao Cu–S–Fe–Au deposit in the Middle-Lower Yangtze valley. Ore Geol. Rev. 43 (1), 194–202.
Wang, S.-X., Zhu, X.-K., Song, X.Y., Chen, L.-M., 2012. Fe isotopic characteristics of V–Ti magnetite deposit in Panzhihua area of the Sichuan province and their genetic implications. Acta Geosci. Sin. 33 (6), 995–1004 (in Chinese with English abstract).
Weyer, S., Ionov, D.A., 2007. Partial melting and melt percolation in the mantle: the message from Fe isotopes. Earth Planet. Sci. Lett. 259 (1–2), 119–133.
Weyer, S., Seitz, H.M., 2012. Coupled lithium- and iron isotope fractionation during magmatic differentiation. Chem. Geol. 294–295, 42–50.
Williams, H.M., Peslier, A.H., McCammon, C., Halliday, A.N., Levasseur, S., Teutsch, N., Burg, J.P., 2005. Systematic iron isotope variations in mantle rocks and minerals: the effects of partial melting and oxygen fugacity. Earth Planet. Sci. Lett. 235 (1–2), 435–452.
Williams, H.M., Nielsen, S.G., Renac, C., Griffin, W.L., O'Reilly, S.Y., McCammon, C.A., Pearson, N., Viljoen, F., Alt, J.C., Halliday, A.N., 2009. Fractionation of oxygen and iron isotopes by partial melting processes: implications for the interpretation of stable isotope signatures in mafic rocks. Earth Planet. Sci. Lett. 283 (1–4), 156–166.
Wombacher, F., Eisenhauer, A., Heuser, A., Weyer, S., 2009. Separation of Mg, Ca and Fe from geological reference materials for stable isotope ratio analyses by MC–ICP–MS and double-spike TIMS. J. Anal. At. Spectrom. 24 (5), 627–636.
Xiao, Y., Teng, F.Z., Zhang, H.F., Yang, W., 2013. Large magnesium isotope fractionation in peridotite xenoliths from eastern North China craton Product of melt–rock interaction. Geochim. Cosmochim. Acta 115, 241–261.
Xu, Y.G., Chung, S.L., Jahn, B.M., Wu, G.Y., 2001. Petrologic and geochemical constraints on the petrogenesis of Permian–Triassic Emeishan flood basalts in southwestern China. Lithos 58 (3–4), 145–168.
Xu, Y.G., He, B., Chung, S.L., Menzies, M.A., Frey, F.A., 2004. Geologic, geochemical, and geophysical consequences of plume involvement in the Emeishan flood-basalt province. Geology 32 (10), 917–920.
Young, E.D., Galy, A., Nagahara, H., 2002. Kinetic and equilibrium mass-dependent isotope fractionation laws in nature and their geochemical and cosmochemical significance. Geochim. Cosmochim. Acta 66 (6), 1095–1104.
Zhang, X.-Q., 2013. Petrogenesis and Fe–Ti Oxide Mineralization of the Baima Layered Intrusion in the Panxi area, SW China. The University of Chinese Academy of Sciences, Institute of Geochemistry, Chinese Academy of Sciences, Guiyang.
Zhang, Z.C., Mahoney, J.J., Mao, J.W., Wang, F.H., 2006. Geochemistry of picritic and associated basalt flows of the western Emeishan flood basalt province, China. J. Petrol. 47 (10), 1997–2019.
Zhang, X.-Q., Song, X.-Y., Chen, L.-M., Xie, W., Yu, S.-Y., Zheng, W.-Q., Deng, Y.-F., Zhang, J.-F., Gui, S.-G., 2012. Fractional crystallization and the formation of thick Fe–Ti–V oxide layers in the Baima layered intrusion, SW China. Ore Geol. Rev. 49, 96–108.
Zhang, X.-Q., Song, X.-Y., Chen, L.-M., Yu, S.-Y., Xie, W., Deng, Y., Zhang, J.-F., Gui, S.-G., 2013. Chalcophile element geochemistry of the Baima layered intrusion, Emeishan Large Igneous Province, SW China: implications for sulfur saturation history and genetic relationship with high-Ti basalts. Contrib. Mineral. Petrol. 166 (1), 193–209.
Zhao, X.M., Zhang, H.F., Zhu, X.K., Tang, S.H., Tang, Y.J., 2010. Iron isotope variations in spinel peridotite xenoliths from North China Craton: implications for mantle metasomatism. Contrib. Mineral. Petrol. 160 (1), 1–14.
Zhao, X.M., Zhang, H.F., Zhu, X.K., Tang, S.H., Yan, B., 2012. Iron isotope evidence for multistage melt-peridotite interactions in the lithospheric mantle of eastern China. Chem. Geol. 292, 127–139.
Zhong, H., Zhu, W.-G., 2006. Geochronology of layered mafic intrusions from the Pan-Xi area in the Emeishan large igneous province, SW China. Mineral. Deposita 41 (6), 599–606.
Zhong, H., Yao, Y., Prevec, S.A., Wilson, A.H., Viljoen, M.J., Viljoen, R.P., Liu, B.-G., Luo, Y.-N., 2004. Trace-element and Sr–Nd isotopic geochemistry of the PGE-bearing Xinjie layered intrusion in SW China. Chem. Geol. 203 (3–4), 237–252.
Zhong, H., Zhu, W.-G., Chu, Z.-Y., He, D.-F., Song, X.-Y., 2007. Shrimp U–Pb zircon geochronology, geochemistry, and Nd–Sr isotopic study of contrasting granites in the Emeishan large igneous province, SW China. Chem. Geol. 236 (1–2), 112–133.

Zhong, H., Qi, L., Hu, R.-Z., Zhou, M.-F., Gou, T.-Z., Zhu, W.-G., Liu, B.-G., Chu, Z.-Y., 2011. Rhenium–osmium isotope and platinum-group elements in the Xinjie layered intrusion, SW China: implications for source mantle composition, mantle evolution, PGE fractionation and mineralization. Geochim. Cosmochim. Acta 75 (6), 1621–1641.

Zhou, M.F., Malpas, J., Song, X.Y., Robinson, P.T., Sun, M., Kennedy, A.K., Lesher, C.M., Keays, R.R., 2002. A temporal link between the Emeishan large igneous province (SW China) and the end-Guadalupian mass extinction. Earth Planet. Sci. Lett. 196 (3–4), 113–122.

Zhou, M.F., Robinson, P.T., Lesher, C.M., Keays, R.R., Zhang, C.J., Malpas, J., 2005. Geochemistry, petrogenesis and metallogenesis of the Panzhihua gabbroic layered intrusion and associated Fe–Ti–V oxide deposits, Sichuan Province, SW China. J. Petrol. 46 (11), 2253–2280.

Zhou, M.F., Arndt, N.T., Malpas, J., Wang, C.Y., Kennedy, A.K., 2008. Two magma series and associated ore deposit types in the Permian Emeishan large igneous province, SW China. Lithos 103 (3–4), 352–368.

Zhu, X.K., Guo, Y., O'Nions, R.K., Young, E.D., Ash, R.D., 2001. Isotopic homogeneity of iron in the early solar nebula. Nature 412 (6844), 311–313.

Zhu, X.K., Guo, Y., Williams, R.J.P., O'Nions, R.K., Matthews, A., Belshaw, N.S., Canters, G.W., de Waal, E.C., Weser, U., Burgess, B.K., Salvato, B., 2002. Mass fractionation processes of transition metal isotopes. Earth Planet. Sci. Lett. 200 (1–2), 47–62.

Zhu, X.-K., Li, Z.-H., Zhao, X.-M., Tang, S.-H., He, X.-X., Belshaw, N.S., 2008. High-precision measurements of Fe isotopes using MCICP-MS and Fe isotope compositions of geological reference materials. Acta Petrol. Mineral. 27 (4), 263–272.